

# Microscopic Dynamics of $\text{Li}^+$ in Rutile $\text{TiO}_2$ Revealed by $^8\text{Li}$ $\beta$ -detected NMR

Ryan M. L. McFadden,<sup>1,2,\*</sup> Terry J. Buck,<sup>3</sup> Aris Chatzichristos,<sup>2,3</sup> Chia-Chin Chen,<sup>4</sup> David L. Cortie,<sup>1,2,3,†</sup> Kim H. Chow,<sup>5</sup> Martin H. Dehn,<sup>2,3</sup> Victoria L. Karner,<sup>1,2</sup> Dimitrios Koumoulis,<sup>6,‡</sup> C. D. Philip Levy,<sup>7</sup> Chilin Li,<sup>8</sup> Iain McKenzie,<sup>7,9</sup> Rotraut Merkle,<sup>4</sup> Gerald D. Morris,<sup>7</sup> Matthew R. Pearson,<sup>7</sup> Zaher Salman,<sup>10</sup> Dominik Samuelis,<sup>4,§</sup> Monika Stachura,<sup>7</sup> Jiyu Xiao,<sup>1</sup> Joachim Maier,<sup>4</sup> Robert F. Kiefl,<sup>2,3,7</sup> and W. Andrew MacFarlane<sup>1,2,7,¶</sup>

<sup>1</sup>*Department of Chemistry, University of British Columbia,  
2036 Main Mall, Vancouver, BC V6T 1Z1, Canada*

<sup>2</sup>*Stewart Blusson Quantum Matter Institute, University of British Columbia,  
2355 East Mall, Vancouver, BC V6T 1Z4, Canada*

<sup>3</sup>*Department of Physics and Astronomy, University of British Columbia,  
6224 Agricultural Road, Vancouver, BC V6T 1Z1, Canada*

<sup>4</sup>*Max-Planck-Institut für Festkörperforschung, Heisenbergstraße 1, 70569 Stuttgart, Germany*

<sup>5</sup>*Department of Physics, University of Alberta, 4-181 CCIS, Edmonton, AB T6G 2E1, Canada*

<sup>6</sup>*Department of Chemistry and Biochemistry, University of California,  
Los Angeles, 607 Charles E. Young Drive East, Los Angeles, CA 90095, USA*

<sup>7</sup>*TRIUMF, 4004 Wesbrook Mall, Vancouver, BC V6T 2A3, Canada*  
<sup>8</sup>*Shanghai Institute of Ceramics, Chinese Academy of Sciences,  
1295 Dingxi Road, Shanghai, P.R. China 200050*

<sup>9</sup>*Department of Chemistry, Simon Fraser University,  
8888 University Drive, Burnaby, BC V5A 1S6, Canada*

<sup>10</sup>*Laboratory for Muon Spin Spectroscopy, Paul Scherrer Institute, CH-5232 Villigen PSI, Switzerland*  
(Dated: August 11, 2018)

We report measurements of the dynamics of isolated  $^8\text{Li}^+$  in single crystal rutile  $\text{TiO}_2$  using  $\beta$ -detected NMR. From spin-lattice relaxation and motional narrowing, we find two sets of thermally activated dynamics: one below 100 K; and one at higher temperatures. At low temperature, the activation barrier is 26.8(6) meV with prefactor  $1.23(5) \times 10^{10} \text{ s}^{-1}$ . We suggest this is unrelated to  $\text{Li}^+$  motion, and rather is a consequence of electron polarons in the vicinity of the implanted  $^8\text{Li}^+$  that are known to become mobile in this temperature range. Above 100 K,  $\text{Li}^+$  undergoes long-range diffusion as an isolated uncompensated cation, characterized by an activation energy and prefactor of 0.32(2) eV and  $1.0(5) \times 10^{16} \text{ s}^{-1}$ , in agreement with macroscopic diffusion measurements. These results in the dilute limit from a microscopic probe indicate that  $\text{Li}^+$  concentration does not limit the diffusivity even up to high concentrations, but that some key ingredient is missing in the calculations of the migration barrier. The anomalous prefactors provide further insight into both  $\text{Li}^+$  and polaron motion.

## I. INTRODUCTION

The mobility of lithium ions inserted into rutile  $\text{TiO}_2$  is exceptionally high and unmatched by any other interstitial cation.<sup>1</sup> Even at 300 K, the  $\text{Li}^+$  diffusion coefficient is as large as  $10^{-6} \text{ cm}^2 \text{ s}^{-1}$ ,<sup>2</sup> exceeding many state-of-the-art solid-state lithium electrolytes.<sup>3,4</sup> Moreover, this mobility is extremely anisotropic,<sup>2</sup> and rutile is a nearly ideal 1D lithium-ion conductor. This is a consequence of rutile's tetragonal structure,<sup>5</sup> which has open channels along the  $c$ -axis that provide a pathway for fast interstitial diffusion (see Fig. 1). This has, in part, led to a keen interest in using rutile as an electrode in lithium-ion batteries,<sup>6</sup> especially since the advantages of nanosized crystallites were realized.<sup>7</sup> Simultaneously, much effort has focused on understanding the lithium-ion dynamics;<sup>8–18</sup> however, many underlying details in these studies are inconsistent with available experimental data. For example, a small activation energy of around 50 meV is consistently predicted,<sup>8–10,12,14–18</sup> but measured barriers are greater by an order of magnitude.<sup>2,19,20</sup> This disagreement is troubling considering the simplicity of both the rutile lattice and the associated  $\text{Li}^+$  motion. One

explanation for the discrepancy is that most experimental methods sense the macroscopic ion transport, while theory focuses on elementary microscopic motion. The two would only be related if the macroscopic transport were not strongly influenced by crystal defects, as might be expected due to the highly one-dimensional mobility. Thus, for a direct comparison with theory it is important to have microscopic measurements of the  $\text{Li}^+$  dynamics.

The electronic properties of rutile are also of substantial interest.<sup>21,22</sup> While it is natively a wide band-gap (3 eV) insulator, it can be made an  $n$ -type semiconductor by introducing electrons into vacant titanium  $3d t_{2g}$  orbitals, reducing its valence from 4+ to 3+. This is easily achieved through optical excitation, extrinsic doping, or by oxygen substoichiometry. Rather than occupying delocalized band states, these electrons form small polarons, where the  $\text{Ti}^{3+}$  ion is coupled to a substantial distortion of the surrounding oxygen octahedron. Polaron formation in rutile is not predicted by naive density functional calculations, and to obtain it one must introduce electron interactions.<sup>23</sup> Recently, the polaron has been studied optically<sup>24</sup> and by electron paramagnetic resonance (EPR).<sup>25</sup> Compared to delocalized band elec-

## Rutile TiO<sub>2</sub>

$P4_2/mnm$  (136)

$a = b = 4.593 \text{ \AA}$

$c = 2.959 \text{ \AA}$

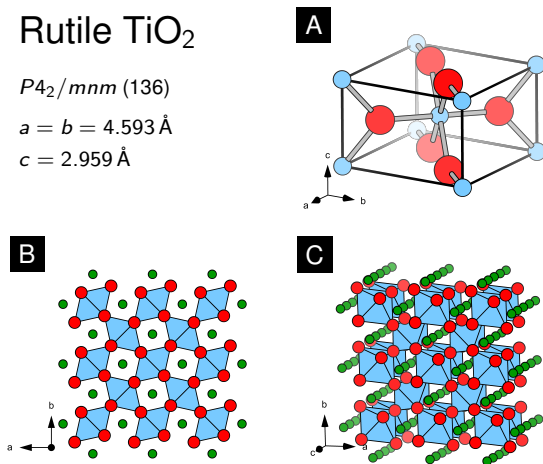


FIG. 1. The rutile structure.<sup>5</sup> (A) Titanium-centred conventional unit cell showing Ti (blue) and oxygen (red) ions. Bonds (grey) are drawn to emphasize coordination. (B) View along the 4-fold  $c$ -axis, revealing the channels for fast interstitial Li<sup>+</sup> diffusion. Lithium (green) are shown in the channel centre ( $4c$  sites) surrounded by the blue Ti-centred octahedra. (C) Off-axis view revealing the 1D channels.

trons, polaron mobility is quite limited and often exhibits thermally activated hopping. Calculations predict that the polaron mobility, like interstitial Li<sup>+</sup>, is also highly anisotropic, with fast transport along the  $c$ -axis stacks of edge sharing TiO<sub>6</sub> octahedra.<sup>12,23,26,27</sup> Importantly for our results, the positive charge of an interstitial cation like Li<sup>+</sup> can bind the polaron into a Li<sup>+</sup>-polaron complex, effectively coupling the electronic and ionic transport.<sup>28</sup> Even before this complex was observed by EPR and electron nuclear double resonance (ENDOR),<sup>29</sup> its effect on the mobility of Li<sup>+</sup> was considered theoretically.<sup>12,30</sup>

To study lithium-ion dynamics in rutile, a technique sensitive to the local environment of Li<sup>+</sup> is desirable. Nuclear magnetic resonance (NMR) is a sensitive microscopic probe of matter with a well-developed toolkit for studying ionic mobility in solids.<sup>31–39</sup> In particular, spin-lattice relaxation (SLR) measurements provide a means of studying fast dynamics. They are sensitive to the temporal fluctuation in the local fields sensed by NMR nuclei, which induce transitions between magnetic sublevels and relax the ensemble of spins towards thermal equilibrium. When these stochastic fluctuations induced by, for example, ionic diffusion, have a Fourier component at the Larmor frequency (typically on the order of MHz)

$$\omega_L = 2\pi\nu_L = 2\pi\gamma B_0, \quad (1)$$

where  $\gamma$  is the gyromagnetic ratio of the NMR nucleus and  $B_0$  is the applied magnetic field, the SLR rate  $\lambda = 1/T_1$  is maximized. Complementary information can be obtained from motion induced changes to the resonance lineshape. In the low temperature limit, the static NMR lineshape is characteristic of the lattice site,

with features such as the quadrupolar splitting and magnetic dipolar broadening from the nuclei of neighboring atoms. As temperature increases and the hop rate exceeds the characteristic frequency of these spectral features, dynamic averaging yields substantially narrowed spectra with sharper structure. This phenomenon is collectively known as “motional narrowing” and is sensitive to slow motion with rates typically on the order of kHz. Together, SLR and resonance methods can provide direct access to atomic hop rates over a dynamic range up to nearly 6 decades.

Here, we use  $\beta$ -detected NMR ( $\beta$ -NMR)<sup>40,41</sup> to measure the Li<sup>+</sup> dynamics in rutile. Short-lived <sup>8</sup>Li<sup>+</sup> ions are implanted at low-energies ( $\sim 20$  keV) into single crystals of rutile, and their NMR signals are obtained by monitoring the <sup>8</sup>Li nuclear spin-polarization through the anisotropic  $\beta$ -decay.  $1/T_1$  measurements reveal two sets of thermally activated dynamics: one low-temperature process below 100 K and another at higher temperatures. The dynamics at high temperature is due to long-range Li<sup>+</sup> diffusion, in agreement with macroscopic diffusion measurements, and corroborated by motional narrowing of the resonance lineshape. We find a dilute-limit activation barrier of 0.32(2) eV, which is consistent with macroscopic diffusivity, but inconsistent with theory. We suggest that the dynamics below 100 K and its much smaller activation barrier are related to the low-temperature kinetics of dilute electron polarons.

The paper is organized as follows: Section II details the methods used. The results of spin lattice relaxation and resonance measurements and their analysis form section III A and III B, respectively. A detailed discussion including comparison to the extensive literature is presented in section IV, and a summary is given in section V. The appendices give some further detail on the spin lattice relaxation model (Appendix A) and on the candidate site for interstitial Li<sup>+</sup> (Appendix B).

## II. EXPERIMENT

$\beta$ -NMR experiments were performed at TRIUMF in Vancouver, Canada. A low-energy  $\sim 20$  keV hyperpolarized beam of <sup>8</sup>Li<sup>+</sup> was implanted into rutile single crystals mounted in one of two dedicated spectrometers.<sup>41–44</sup> The incident ion beam has a typical flux of  $\sim 10^6$  ions/s over a beam spot  $\sim 3$  mm in diameter. At these implantation energies, the <sup>8</sup>Li<sup>+</sup> stop at average depths of at least 100 nm,<sup>45</sup> as calculated by the SRIM Monte Carlo code.<sup>46</sup> Spin-polarization was achieved in-flight by collinear optical pumping with circularly polarized light, yielding a polarization of  $\sim 70\%$ .<sup>47</sup> The samples are one-side epitaxially polished (roughness  $< 0.5$  nm), commercial substrates with typical dimensions  $8 \times 10 \times 0.5$  mm<sup>3</sup> (Crystal GmbH, Berlin). All the samples were transparent to visible light, but straw-coloured, qualitatively indicating a minor oxygen deficiency.<sup>48</sup> The probe nucleus, <sup>8</sup>Li, has nuclear spin  $I = 2$ , gyromagnetic ratio

$\gamma = 6.3016 \text{ MHz T}^{-1}$ , nuclear electric quadrupole moment  $Q = +32.6 \text{ mb}$ , and radioactive lifetime  $\tau_\beta = 1.21 \text{ s}$ .

In all the  $\beta$ -NMR measurements, the nuclear spin-polarization of  $^8\text{Li}$  is monitored through its anisotropic  $\beta$ -decay, and the observed *asymmetry* of the  $\beta$ -emissions is proportional to the average longitudinal nuclear spin-polarization.<sup>40,41</sup> The proportionality factor,  $A_0$ , is determined by the  $\beta$ -decay properties of  $^8\text{Li}$  and the detection geometry of each experiment.

SLR measurements were performed by monitoring the transient decay of spin-polarization both during and following a short pulse of the  $^8\text{Li}^+$  beam.<sup>49,50</sup> During the pulse, the polarization approaches a steady-state value, while following the pulse, it relaxes to  $\sim 0$ . This produces a pronounced kink at the end of the beam pulse, characteristic of  $\beta$ -NMR SLR spectra (see Fig. 2). Note that no radio-frequency (RF) field is required for the SLR measurements, as the probe spins are implanted in a spin state already far from equilibrium. As a result, just opposite to conventional NMR, it is faster and easier to measure SLR than to measure the resonance, but as a corollary, this type of relaxation measurement has no spectral resolution. It represents the spin relaxation of *all* the  $^8\text{Li}$  in the sample, not only those corresponding to measurable resonances. SLR rates in rutile were measured from 5–300 K under applied magnetic fields of: 1.90 T and 6.55 T parallel to the  $\text{TiO}_2$  (100); and 10 mT and 20 mT perpendicular to the  $\text{TiO}_2$  (100).

In a continuous  $^8\text{Li}^+$  beam, resonances were acquired in the high-field spectrometer<sup>44</sup> with a continuous wave (CW) transverse RF magnetic field stepped slowly through the  $^8\text{Li}$  Larmor frequency. The spin of any on-resonance  $^8\text{Li}$  is precessed rapidly by the RF field, resulting in a loss in time-averaged asymmetry. The evolution of the resonance was recorded over a temperature range of 10 K to 315 K with a highly-homogeneous magnetic field of 6.55 T parallel to the  $\text{TiO}_2$  (100). The resonance frequency was calibrated against that in single crystal  $\text{MgO}$  (100) at 300 K,<sup>51</sup> with the superconducting solenoid persistent. A typical relaxation measurement takes about 20 min, while a resonance measurement requires about 1 h.

### III. RESULTS AND ANALYSIS

#### A. Spin-Lattice Relaxation

Typical SLR data at high and low field are shown in Fig. 2 for several temperatures. In high magnetic fields, the relaxation is remarkably fast compared to other oxide insulators,<sup>51–53</sup> consistent with an earlier report in an intermediate field of 0.5 T.<sup>54</sup> It is also immediately evident that the SLR rates are strongly dependent on both temperature and field. The rate of relaxation increases monotonically as the magnetic field is decreased towards zero, see Fig. 2. At fixed field, however, the temperature dependence of the relaxation is *nonmonotonic*, and

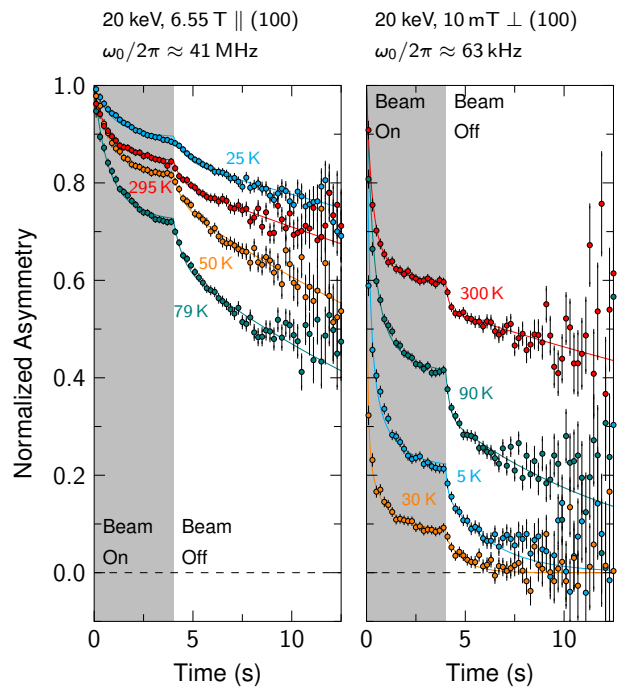


FIG. 2. SLR spectra of  $^8\text{Li}^+$  in rutile with  $B_0 = 6.55 \text{ T} \parallel (100)$  [left] and  $10 \text{ mT} \perp (100)$  [right]. The relaxation becomes faster with decreasing magnetic field and is a non-monotonic function of temperature. The solid lines are a fit to biexponential relaxation function [Eq. (2)] convoluted with a 4 s square beam pulse.<sup>49,50</sup> These fit curves were obtained from a global fitting procedure where a temperature independent overall amplitude  $A_0$  is shared for all spectra at each field, as described in the text. The spectra have been binned by a factor of 20 for clarity.

there is at least one temperature where the relaxation rate is locally maximized. Moreover, the temperature of the relaxation rate peak is field-dependent, increasing monotonically with increasing field.

To make these observations quantitative, we now consider a detailed analysis. The relaxation is not single exponential at *any* field or temperature, but a phenomenological biexponential relaxation function, composed of fast and slow relaxing components yields a good fit. For an  $^8\text{Li}^+$  ion implanted at time  $t'$ , the spin polarization at time  $t > t'$  follows:<sup>49,50</sup>

$$R(t, t') = f_{\text{slow}} e^{-\lambda_{\text{slow}}(t-t')} + (1 - f_{\text{slow}}) e^{-\lambda_{\text{fast}}(t-t')}, \quad (2)$$

where the rates are  $\lambda_{\text{fast/slow}} = 1/T_1^{\text{fast/slow}}$ , and  $f_{\text{slow}} \in [0, 1]$  is the slow relaxing fraction. We discuss possible origins for biexponential  $R(t, t')$  in Appendix A.

With this model, all the data at each field are fit simultaneously with a shared common initial asymmetry ( $A_0$ ) using the MINUIT<sup>55</sup> minimization routines within ROOT<sup>56</sup> to find the optimum global nonlinear least-squares fit. Notice that the statistical error bars are highly *inhomogeneous* with time, characteristic of the radioactive  $^8\text{Li}$  decay. During the beam pulse, the un-

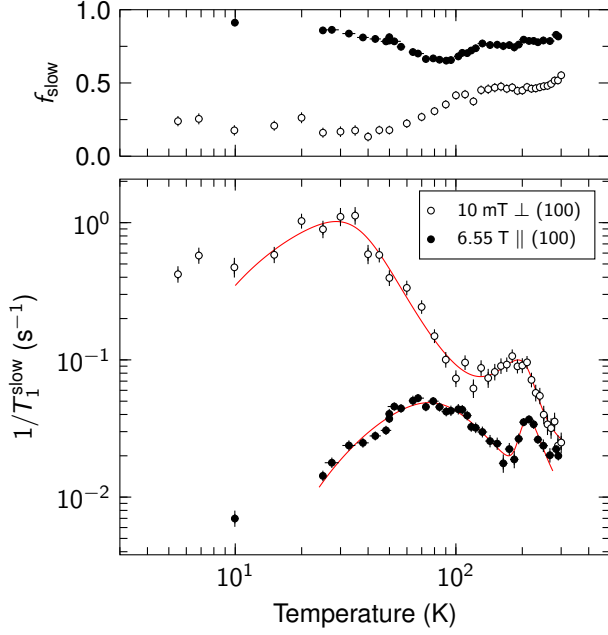


FIG. 3. Results from the analysis of the SLR measurements using Eq. (2) at high- and low-field. Shown are the fraction of the slow relaxing component (top) and the slow relaxation rate (bottom).  $f_{\text{slow}}$  is surprisingly both temperature- and field-dependent, but increases towards 1 by 300 K. The qualitative features of the SLR spectra in Fig. 2 can be seen clearly in the two field-dependent rate maxima in  $1/T_1^{\text{slow}}$ . The solid red line is drawn to guide the eye.

certainly decreases with time as the statistics increase, reaching a minimum at the trailing edge of the 4 s beam pulse. Following the pulse, the error bars grow exponentially as  $\exp(-t/\tau_\beta)$ , e.g. Fig. 2. Accounting for this purely statistical feature of the data is crucial in the analysis. A subset of the results are shown as solid coloured lines in Fig. 2. The fit quality is good in each case (global  $\chi^2 \approx 1.1$ ). The relaxation rates of the two components are very different with  $\lambda_{\text{fast}} > 20\lambda_{\text{slow}}$ , and the analysis distinguishes them clearly.

The main fit results are shown in Fig. 3. Consistent with the qualitative behaviour of the spectra in Fig. 2, the relaxation rate exhibits two maxima at each field. This is most apparent in the slow relaxing component at high magnetic field, while at low field, the low temperature peak is substantially broadened. Generally, a maximum in the relaxation rate occurs when the average fluctuation rate matches the Larmor frequency,<sup>31–39</sup> while the detailed temperature dependence  $\lambda(T)$  depends on the character of the fluctuations.

Though the two relaxing components share similarities in their temperature dependence (Fig. 3 and Appendix A), we emphasize that the *slow* relaxing component is the more reliable. Even though the sample is much larger than the incident ion beam spot, backscattering can result in a small fraction of the  $^8\text{Li}^+$  stopping outside the sample which typically produces a cor-

respondingly small fast relaxing asymmetry.<sup>41</sup> At high field, where  $^8\text{Li}^+$  relaxation is generally slow, most materials show such a fast relaxing component easily distinguishable from the features of interest; however, when quadrupolar relaxation is present, which results in multi-exponential relaxation for high-spin nuclei<sup>57–59</sup> (see Appendix A), distinguishing the background contribution from an intrinsic fast component becomes difficult. At low fields, a background is even harder to isolate as  $^8\text{Li}^+$  relaxation is typically fast under these conditions. Therefore, even though the slow component is a minority fraction at low field (see Fig. 3), we assert that it is the more reliable. The fact that, as discussed in the following sections, we are able to reproduce material properties observed with other techniques is strong confirmation of the appropriateness of this choice.

## B. Resonance

We now turn to the measurements of the  $^8\text{Li}$  resonance spectrum at  $B_0 = 6.55$  T. As expected in a non-cubic crystal, the NMR is split into a multiplet pattern of quadrupole satellites by the interaction between the  $^8\text{Li}$  nucleus and the local electric field gradient (EFG) characteristic of its crystallographic site. As seen in Fig. 4A, the resonance lineshape changes substantially with temperature. At 10 K, it is broad with an overall linewidth of about 40 kHz, near the maximum measurable with the limited amplitude RF field of this broadband spectrometer.<sup>42,44</sup> Some poorly resolved satellite structure is still evident though. As the temperature increases, the intensity of the resonance increases considerably with only limited narrowing. Above 45 K, however, the resonance area decreases dramatically and is minimal near 100 K. As the temperature is raised further, the quadrupolar splitting becomes more evident, especially above 130 K. Moreover, the sharpening of these spectral features coincides with a reduction in the breadth of line, along with another increase in signal intensity. These high-temperature changes are qualitatively consistent with motional narrowing for a mobile species in a crystalline environment. By room temperature, the spectrum is clearly resolved (see Fig. 4B) into the expected pattern of  $2I$  single quantum ( $|\Delta m| = 1$ ) quadrupole satellites interlaced with narrower double quantum transitions. The well-resolved quadrupolar structure indicates a well-defined time-average EFG experienced by a large fraction of the  $^8\text{Li}$  at this temperature. At all temperatures, the centre of mass of the line is shifted to a lower frequency relative to  $^8\text{Li}^+$  in MgO at 300 K. Note that the resonances in Fig. 4 are all normalized to the off-resonance steady state asymmetry, which accounts for all the variation of signal intensity due to spin-lattice relaxation.<sup>60</sup>

The scale of the quadrupolar interaction is the

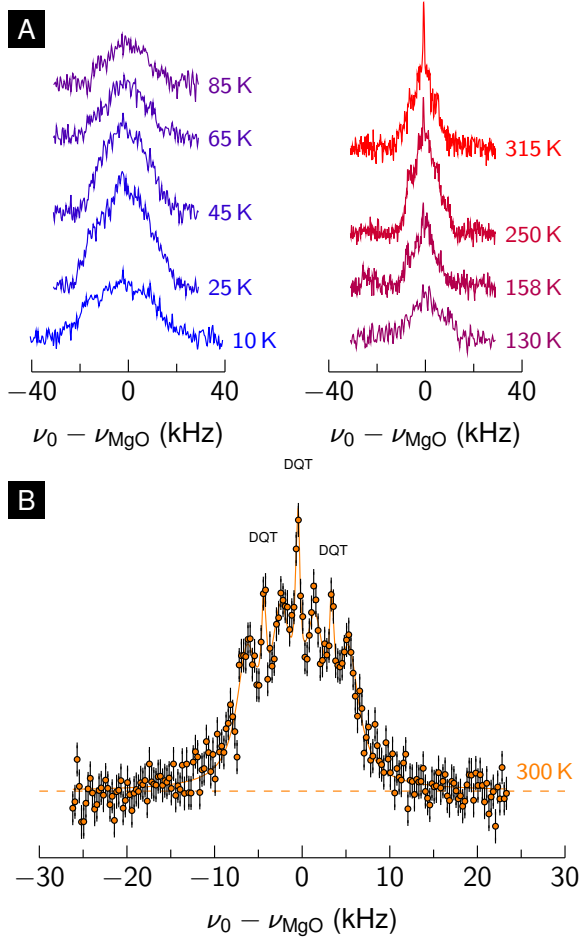


FIG. 4.  $^{8}\text{Li}^+$  resonance in rutile  $\text{TiO}_2$  with 6.55 T  $\parallel$  (100). (A) Temperature dependence of the resonance. Note that both the vertical and horizontal scales are the same for each spectra, which are offset for clarity. The zero-shifted position is taken as the resonance frequency of  $^{8}\text{Li}^+$  in MgO at 300 K. The lineshape changes substantially with temperature. Notice that it is most intense at 25 K, but quickly diminishes as the temperature is raised. At higher temperatures, motional narrowing is apparent and the quadrupolar structure becomes clearly visible. (B) High-resolution spectrum at 300 K. The quadrupolar satellite transitions are clearly visible, including narrow double-quantum transitions (DQTs) [positions indicated by DQT] interlaced between the satellites. The solid orange line is a fit described in the text.

quadrupole frequency:<sup>61</sup>

$$\nu_q = \frac{e^2 q Q}{4h}, \quad (3)$$

where the  $eq$  is the principal component of the EFG tensor. From the spectra, the splitting is on the order of a few kHz, small relative to the Larmor frequency. In this limit, the single quantum satellite positions are given accurately by first order perturbation theory as:<sup>61</sup>

$$\nu_i = \nu_0 - n_i \frac{\nu_q}{2} f(\theta, \phi), \quad (4)$$

where  $n_i = \pm 3(\pm 1)$  for the outer (inner) satellites, and  $f$  is a function of the polar and azimuthal angles  $\theta$  and  $\phi$  between the external field and EFG principal axis system:

$$f(\theta, \phi) = \frac{1}{2} (3 \cos^2 \theta - 1 + \eta \sin^2 \theta \cos 2\phi). \quad (5)$$

Here,  $\eta \in [0, 1]$  is the asymmetry parameter for the EFG, which is zero for axial symmetry. The spectrum thus consists of 4 satellites split symmetrically about  $\nu_0$ . Unlike the more common case of half-integer spin, there is no unshifted “main line” (the  $m = \pm 1/2$  transition). The satellite intensities are also different from conventional NMR, being determined mainly by the high degree of initial polarization that increases the relative amplitude of the outer satellites.<sup>47</sup>

We now consider a detailed analysis of the resonances. In agreement with an earlier report,<sup>45</sup> the anti-symmetry in helicity-resolved spectra<sup>41</sup> reveals the resonance is quadrupole split at *all* temperatures; however, below 100 K the splitting is not well resolved, and an attempt to fit the spectra to a sum of quadrupole satellites proved unsuccessful. Instead, we use a single Lorentzian in this temperature region to approximate the breadth of the line. At higher temperatures, where the satellite lines become sharper, a sum of Lorentzians centred at positions given by Eq. (4) (including interlacing double-quantum transitions close to room temperature)<sup>41</sup> with all  $m$ -quanta satellites sharing the same linewidth. From the fits, we extract: the central frequency  $\nu_0$ ; the quadrupole splittings  $\nu_q$ ; and the overall/satellite linewidths. From  $\nu_0$ , we calculate the frequency shift  $\delta$  relative to  $^{8}\text{Li}^+$  in MgO at 300 K in parts per million (ppm) using:

$$\delta = \frac{\nu_0 - \nu_{\text{MgO}}}{\nu_{\text{MgO}}}. \quad (6)$$

Additionally, the normalized resonance area was estimated following a procedure that removed any effect of SLR on the line intensity using a baseline estimation algorithm.<sup>62</sup> This allowed for a common integration scheme, independent of a particular fit model.

The results of this analysis are shown in Fig. 5. Though the scatter in the quantities extracted are largest near 100 K, where the resonance is weakest, the qualitative trends noted above are evident. At low temperatures, the resonance is both widest and most intense, narrowing only modestly approaching 100 K. The resonance area is clearly largest around 25 K, but quickly diminishes to a minimum around 100 K. At higher temperatures where the quadrupolar structure is better resolved, the satellites have a nearly temperature independent width of  $\sim 4.8$  kHz. The apparent  $\nu_q$  reduces gradually from  $\sim 3.8$  kHz to nearly half that value by 200 K. This reduction in splitting coincides with an increase in area, consistent with the picture of motional averaging of the quadrupolar interaction.<sup>63,64</sup> This implies a fluctuation rate on the order of  $\sim 2 \times 10^4 \text{ s}^{-1}$  by  $\sim 140$  K ( $T_{\text{MN}}$  in Fig. 5). The resonance shift  $\delta$  is both small and negative

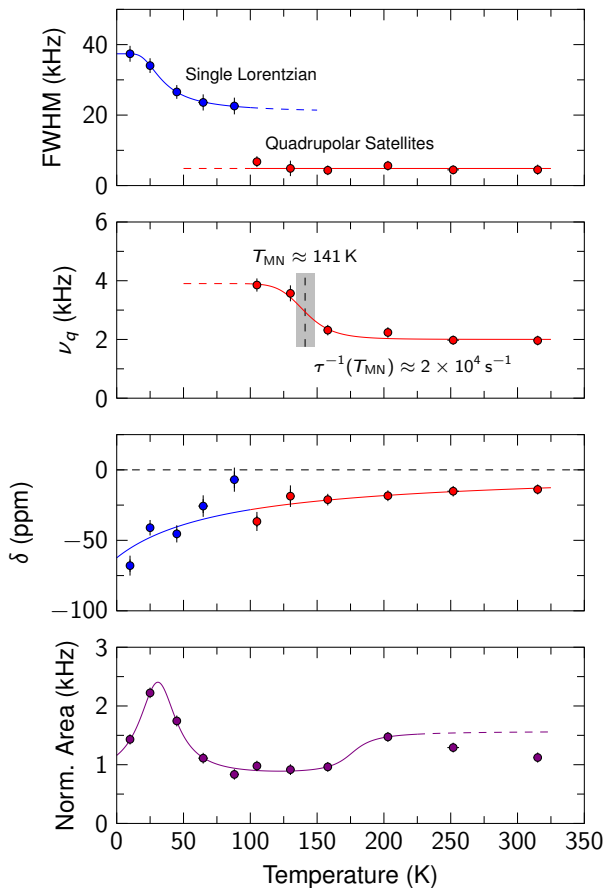


FIG. 5. Results for the analysis of the resonance measurements at high field. Shown (from top to bottom) are the temperature dependence of the: linewidths, quadrupole frequency, resonance shift, and integrated area. In qualitative agreement with the normalized spectra, the resonance is broadest at low temperatures, and gradually reduces in breadth as the temperature is raised. Above 100 K the quadrupole satellites become resolved and their splitting is gradually reduced by a factor of  $\sim 2$  by 200 K. An estimate of the motional narrowing temperature  $T_{MN}$  and an associated hop rate  $\tau^{-1}(T_{MN})$  is indicated. The line is clearly most intense at low temperatures, as indicated by the resonance area, even though it is broadest here.

at all temperatures, gradually increasing towards zero as the temperature is raised.

#### IV. DISCUSSION

The remarkably fast and strongly temperature dependent spin-lattice relaxation at high magnetic field implies an exceptional relaxation mechanism for  $^8\text{Li}$  in rutile distinct from other oxide insulators.<sup>51–53</sup> The occurrence of a  $T_1$  minimum indicates some spontaneous fluctuations are present that are: 1) coupled to the nuclear spin; and 2) their characteristic rate sweeps through the NMR frequency at the temperature of the minimum. Diffusive

motion of  $^8\text{Li}^+$  through the lattice provides at least one potential source of such fluctuations, as is well established in conventional NMR;<sup>31–39</sup> however, without assuming anything about the particular fluctuations, we extract the temperatures  $T_{\min}$  of the two  $T_1$  minima (see Fig. 3), by simple parabolic fits, at several magnetic fields corresponding to NMR frequencies spanning three orders of magnitude. This approach has the advantage of not relying on any particular form of the NMR spectral density function  $J(\omega_L)$ ,<sup>65</sup> which is proportional to  $1/T_1$ . Note that there is a clear field dependence to the high-temperature flanks of the  $T_1$  minima in Fig. 3 (i.e., they do not coalesce at high temperatures). This indicates that the fluctuations are not the result of a 3D isotropic process,<sup>31</sup> but rather one that is spatially confined to lower dimensions.<sup>32,66</sup> Note that for a 1D process (as might be expected in rutile), one needs to account for the characteristic non-Debye fluctuation spectrum,<sup>67,68</sup> where only the asymptotic form is known.<sup>32,66</sup>

Identifying the inverse correlation time of the fluctuations  $\tau^{-1}(T_{\min})$  with the NMR frequency  $\omega_L$  [Eq. (1)], we construct an Arrhenius plot of the average fluctuation rate in Fig. 6. The value of this approach is evident in the linearity of the results which indicates two independent types of fluctuations each with a characteristic activated temperature dependence. To this plot, we add the estimate of the fluctuation rate causing motional narrowing of the resonance spectra (see  $\nu_q(T)$  in Fig. 5), where  $\tau^{-1}(T_{MN})$  matches the static splitting of the line, further expanding the range of  $\tau^{-1}$ . That this point lies along the steeper of the two lines is a strong confirmation that the same fluctuations responsible for the high temperature  $T_1$  minimum cause the motional narrowing. Linear fits to a simple Arrhenius relationship,

$$\tau^{-1} = \tau_0^{-1} e^{-E_A/(k_B T)}, \quad (7)$$

where  $T$  is the temperature,  $k_B$  the Boltzmann constant,  $E_A$  the activation energy, and  $\tau_0^{-1}$  the prefactor, yield:  $\tau_0^{-1} = 1.23(5) \times 10^{10} \text{ s}^{-1}$  and  $E_A = 26.8(6) \text{ meV}$  for the shallow slope, low-temperature fluctuations; and  $\tau_0^{-1} = 1.0(5) \times 10^{16} \text{ s}^{-1}$  and  $E_A = 0.32(2) \text{ eV}$  for the steep high temperature fluctuations.

The motional narrowing above 100 K is clear evidence that the corresponding fluctuations are due to long-range diffusive motion of  $^8\text{Li}^+$ . Unlike liquids, where motion causes the broad solid state lines to collapse to a single narrow Lorentzian, fast interstitial diffusion in a crystal averages only some of the features of the lineshape, e.g., see the  $^7\text{Li}$  spectra in  $\text{Li}_3\text{N}$ .<sup>69</sup> In particular, since the quadrupole splitting (the major spectral feature of the  $^8\text{Li}$  resonance in rutile), is finite at every site, fast motion between sites results in an averaged lineshape consisting of quadrupole satellites split by an average EFG of reduced magnitude, see Fig. 4. From this we conclude that the rate  $\tau^{-1}$  for the steep high temperature fluctuations in Fig. 6 should be identified with the rate of activated hopping of  $^8\text{Li}^+$  between adjacent sites — the elementary atomic process of diffusion in a crystal lattice. Further

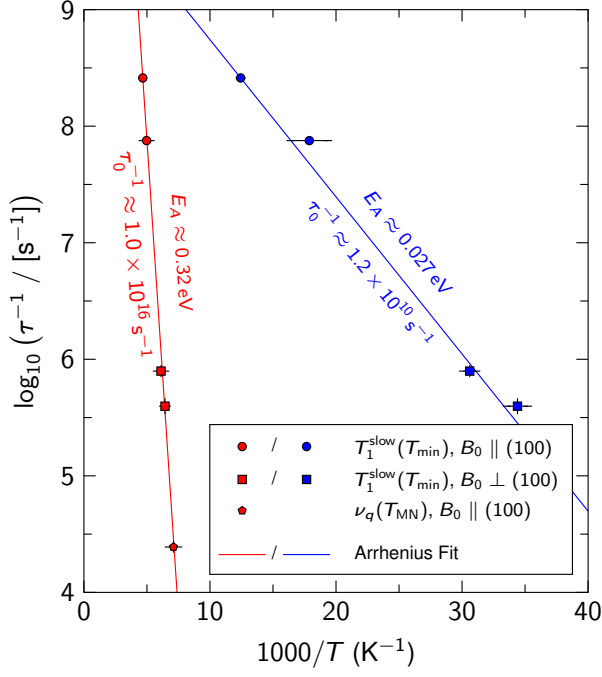


FIG. 6. Arrhenius plot of the fluctuation rate extracted from  $^8\text{Li}$   $\beta$ -NMR SLR and resonance measurements. Two thermally activated processes can be identified: one below 100 K with a shallow slope (blue points); and one at higher temperatures with a steep slope (red points). The solid lines are fits to Eq. (7) with the activation energies and prefactors indicated.

confirmation of this identification comes from the excellent agreement of the activation energy with macroscopic diffusion measurements based on optical absorption<sup>2</sup> and impedance spectroscopy.<sup>19</sup>

For a closer comparison with these experiments, we convert our hop rates to diffusivity via the Einstein-Smolouchouski expression:

$$D = f \frac{l^2}{2d\tau}, \quad (8)$$

where  $l$  is the jump distance,  $d = 1$  is the dimensionality, and  $f$  is the correlation factor, assumed to be unity for direct interstitial diffusion. Using  $l \approx 1.5 \text{ \AA}$ , based on the ideal rutile lattice (details of the precise site of  $^8\text{Li}^+$  are discussed below), and compare the results to  $D$  measured by other methods in single crystal,<sup>2</sup> thin film,<sup>70,71</sup> and nanocrystalline<sup>19</sup> rutile in Fig. 7. The agreement in activation energy is apparent in the similarity of the slopes, but our  $D$  is somewhat larger than the macroscopic diffusivity due to a larger prefactor. In our measurements  $^8\text{Li}^+$  is essentially in the dilute limit, while the bulk measurements have much higher concentrations. One might expect repulsive  $\text{Li}^+ - \text{Li}^+$  interactions would inhibit ionic transport, and yield a smaller macroscopic  $D$ ; however, the agreement in  $E_A$  with the macroscopic  $D$ , where the (Li/Ti) concentration is as high as 30%,<sup>19</sup> implies the barrier is very insensitive to concentration, probably due

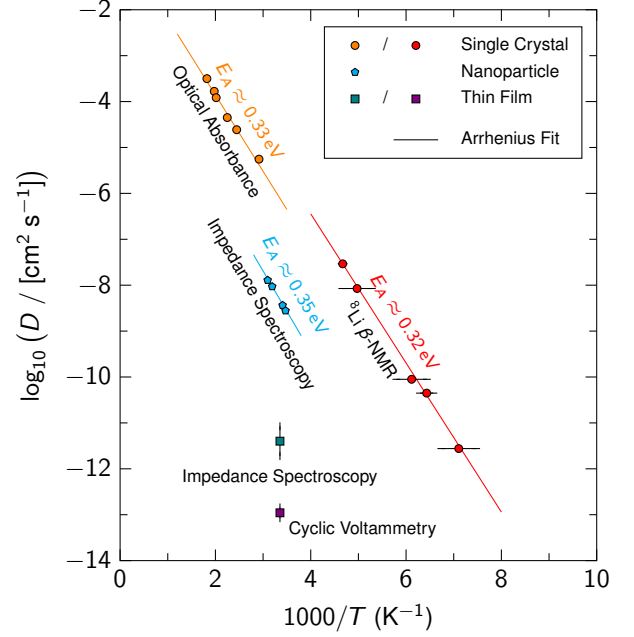


FIG. 7. Arrhenius plot of the  $\text{Li}^+$  diffusion coefficient in rutile estimated from the  $^8\text{Li}^+$  hop rate extracted in Fig. 6 using the Einstein-Smolouchouski expression [Eq. (8)] with  $f = 1$ ,  $d = 1$ , and  $l = 1.5 \text{ \AA}$ . Literature values obtained from rutile single crystals,<sup>2</sup> nanoparticles,<sup>19</sup> and thin films<sup>70,71</sup> are shown for comparison. Note that the concentration of lithium varies greatly in the reported values. While a clear deviation in the magnitude of  $D$  is observed for different forms of rutile, the similarity of  $E_A$  implies a common diffusion mechanism.

to strong screening of the Coulomb interaction by the high dielectric response of rutile.<sup>72</sup> Alternatively, Eq. (8) shows that either overestimating the jump distance  $l$  or the presence of correlated hopping (that reduces  $f$  from unity)<sup>73</sup> would lead to an overestimate of  $D$  and might account for some of the discrepancy. Note that isotopic mass effects on  $D$  are expected to be negligible.<sup>74</sup>

While our  $E_A$  agrees well with macroscopic measurements,<sup>2,19</sup> it disagrees with theory by nearly an order of magnitude.<sup>8-18</sup> Generally  $E_A$  is a more robustly determined quantity than the absolute value of  $D$  at a single temperature, which may exhibit dependence on both sample<sup>2</sup> and measurement technique, e.g., Fig. 7. Moreover, several calculations also predict a strong  $E_A$  dependence on  $\text{Li}^+$  concentration,<sup>11,14,16</sup> inconsistent with our results. While a concentration dependence to  $D$  has been observed,<sup>2,19</sup> it must find an explanation other than a change in  $E_A$ . From this we conclude that some ingredient is missing in the theoretical treatments, possibly related to the lattice relaxation around interstitial  $\text{Li}^+$  that has a strong effect on the calculated barrier.<sup>9,10</sup> Our result is also inconsistent with the suggestion<sup>12</sup> that the higher barrier is characteristic of diffusion of the  $\text{Li}^+$ -polaron complex instead of simply interstitial  $\text{Li}^+$ . We discuss this point at more length below.

We turn now to the fluctuations that predominate be-

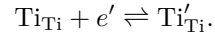
low 100 K and cause the low temperature  $T_1$  minimum. While, we cannot be as conclusive about their origin, we delineate some interesting possibilities. In contrast to the long-range diffusive behaviour at higher temperature, the small activation energy we find is in the range of barriers obtained from molecular dynamics<sup>12,14,15,18</sup> and density functional<sup>8–10,14,16,17</sup> calculations for interstitial  $\text{Li}^+$ ; however, this appears to be coincidental, since the absence of motional narrowing in this temperature range is inconsistent with long-range motion.

On the other hand, the relaxation may be caused by some highly localized  $\text{Li}^+$  motion at low temperature. Local dynamics of organic molecules in solids are well-known, for example the rotation of methyl groups of molecules intercalated into crystalline hosts, where they can cause some limited dynamic averaging of the NMR lineshape<sup>63</sup> and relaxation.<sup>75</sup> Analogous effects are found for some point defects in crystals. For example, a small substitutional cation may adopt one of several equivalent off-centre sites surrounding the high symmetry site of the large missing host cation, and subsequently hop randomly among these sites within the anionic cage, e.g.,  $\text{Ag}^+$  in  $\text{RbCl}$ .<sup>33</sup>

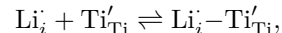
To expand further on this possibility, we now consider the  $^8\text{Li}^+$  site in rutile in more detail. When Li is introduced either thermally or electrochemically, it is known to occupy the open channels along the  $c$ -axis. Two high-symmetry sites are available here: the Wyckoff  $4c$  site within a distorted oxygen octahedron; and the  $4d$  quasi-tetrahedral site, but the precise location remains controversial and may depend on Li concentration.<sup>7,76,77</sup> Although ion implantation is far from a thermal process, the implanted ion often stops in the most energetically stable site in the unit cell. From first-principles, the lowest energy site for isolated  $\text{Li}^+$  is  $4c$  along the centre of the  $c$ -axis channel,<sup>12,14,16,17</sup> see Fig. 1B and C. In disagreement with these calculations, an off-centre site near  $4c$  has been predicted,<sup>8–10</sup> but this seems unlikely given the modest size of the quasi-octahedral cage compared to the  $\text{Li}^+$  ionic radius.<sup>78</sup> Metastable sites outside the channels (in the stacks of  $\text{TiO}_6$  octahedra) have substantially higher energies<sup>8–10,18</sup> and would also be characterized by much larger EFGs and quadrupole splittings (in Appendix B, we consider the prospects for using the quadrupole splitting to *determine* the  $^8\text{Li}^+$  site). If, on the other hand,  $^8\text{Li}^+$  stops at a metastable site along the channels, such as  $4d$ , it would have a very small barrier to moving to the nearest  $4c$  site. Thus, while we cannot rule out some local motion of  $^8\text{Li}^+$  at low temperature, we regard it as unlikely. Moreover, it is not clear how local motion could account for the temperature evolution of the resonance area, whose main feature is a peak in intensity below 50 K, see Fig. 4.

We now consider another source of low  $T$  fluctuations, namely the electron polaron, which, for simplicity, we denote as  $\text{Ti}'_{\text{Ti}}$ . The polaron is only slightly lower in energy (0.15 eV) than the delocalized electronic state ( $e'$ ) at the bottom of the rutile conduction band.<sup>21,26</sup> We can

write the localization transition as:



Having localized, the polaron can migrate in an activated manner, with a calculated  $E_A$  that may be as low as  $\sim 30$  meV for adiabatic hopping along the  $c$ -axis stacks of  $\text{TiO}_6$  octahedra.<sup>12,23,26,27</sup> Note that polaron localization also results in the formation of a local electronic magnetic moment — the polaron is a *paramagnetic defect* — as is clearly confirmed by EPR.<sup>25</sup> At low temperature, the polaron is likely weakly bound to other defects such as an oxygen vacancies, from which it is easily freed.<sup>79,80</sup> If the one dimensionally mobile polaron and interstitial  $\text{Li}^+$  on adjacent sublattices come into close proximity, they may form a bound state:



that is a charge-neutral paramagnetic defect complex that has been characterized by EPR and ENDOR.<sup>29</sup> The complex is predicted to be quite stable,<sup>12</sup> but its EPR signal broadens and disappears above about 50 K.<sup>29</sup> The complex is also expected to be mobile via a tandem hopping process.<sup>12</sup>

$^8\text{Li}^+$  bound to a polaron will have a very different NMR spectrum than the isolated interstitial. The  $3+$  charge of the nearby  $\text{Ti}'_{\text{Ti}}$  will alter the EFG and modify the quadrupole splitting, but the magnetic hyperfine field of the unpaired electron spin is an even larger perturbation, so strong in fact, that complexed  $^8\text{Li}^+$  will not contribute at all to the resonances in Fig. 4, since, based on the ENDOR<sup>29</sup> their resonance frequency is shifted by at least 350 kHz. For this reason we also exclude the possibility that the high temperature dynamics corresponds to motion of the  $\text{Li}_i - \text{Ti}'_{\text{Ti}}$  complex. There is no evidence that its spin polarization is wiped out by fast relaxation which would result in a missing fraction in Fig. 2. However, if immediately after implantation the  $^8\text{Li}^+$  is free for a time longer than the period of precession in the RF field ( $\sim 1$  kHz), it will contribute to the resonance before binding with a polaron. Similarly, if the  $\text{Li}_i - \text{Ti}'_{\text{Ti}}$  complex undergoes cycles of binding and unbinding at higher temperature, provided it is unbound for intervals comparable to the precession period, it will participate in the resonance. In analogy with the closely related technique of RF muon spin resonance (RF- $\mu\text{SR}$ ),<sup>81</sup> one can thus use the resonance amplitude of the diamagnetic  $^8\text{Li}^+$  in Fig. 4 to follow kinetic processes involving the implanted ion, e.g., the hydrogenic muonium defect in silicon.<sup>82</sup> Along these lines, we suggest that the nonmonotonic changes in resonance amplitude at low temperature reflect dynamics of the  $\text{Li}^+$ -polaron complexation. The sample in our measurements is nominally undoped, and we expect the main source of polarons is oxygen substoichiometry. From its color,<sup>48</sup> it could have oxygen vacancies at the level of 0.1 % or less and polarons resulting from these vacancies are known to become mobile below 50 K.<sup>79,80</sup> Alternatively, polarons may result from electron-hole excitations created by the implantation of  $^8\text{Li}^+$ .

The large increase in resonance area between 10 and 25 K implies some form of slow dynamics on the timescale of the  $^8\text{Li}$  lifetime  $\tau_\beta$ . This could be a modulation of the EFG, but more likely it is a magnetic modulation related to the polaron moment as it mobilizes. This is not motional narrowing, but rather a slow variation in the resonance condition, such that the applied RF matches the resonance frequency for many more  $^8\text{Li}$  at some point during their lifetime. The increase of intensity then corresponds to the onset of polaron motion, while the loss in intensity with increasing temperature is due to formation of the  $\text{Li}^+$ -polaron complex, and the fluctuations from this motion also become fast enough to produce the  $T_1$  minimum. The complex does not survive to high temperatures, though, and, based on the resonance intensity, the motionally narrowed quadrupolar split resonance at high temperature corresponds to nearly all of the  $^8\text{Li}$ . The  $E_A$  from the low temperature slope in Fig. 6 is remarkably compatible with the thermal instability of the intrinsic (unbound) polaron in rutile,<sup>12,23,25–27,29</sup> consistent with this picture.

Aside from the activation energies, the prefactors  $\tau_0^{-1}$  from Eq. (7) may provide further information on the processes involved. For atomic diffusion, the prefactor is often consistent with a vibrational frequency of the atom in the potential well characteristic of its crystalline site, typically  $10^{12}$ – $10^{13} \text{ s}^{-1}$ . Prefactor *anomalies* refer to any situation where  $\tau_0^{-1}$  falls outside this range.<sup>83</sup> From Fig. 6, we see that  $\tau_0^{-1}$  for the high temperature dynamics is anomalously high, while for the low temperature process it is anomalously low. Within thermodynamic rate theory:<sup>84,85</sup>

$$\tau_0^{-1} = \tilde{\nu}_0 e^{\Delta S/k_B}, \quad (9)$$

where  $\Delta S$  is the entropy of migration,<sup>86</sup> and  $\tilde{\nu}_0$  is the attempt frequency. For closely related processes,  $\Delta S$  is *not* independent of  $E_A$ , giving rise to Meyer-Neldel (enthalpy-entropy) correlations between the Arrhenius slope and intercept,<sup>87–89</sup> but independent of such correlations, a prefactor anomaly may simply result from  $\Delta S/k_B$  being substantially different from 1.

We first consider the high temperature prefactor, noting that the bulk diffusivity also shows an unusually large  $D_0$ .<sup>2</sup> Prefactors of this magnitude are uncommon, but not unprecedented. For example,  $^7\text{Li}$  NMR in LiF at high temperature yields a comparably large  $\tau_0^{-1}$  for vacancy diffusion in the “intrinsic” region.<sup>90</sup> Similarly, a large prefactor is observed from  $^{19}\text{F}$  NMR in superionic  $\text{PbF}_2$ .<sup>91</sup> The latter case was attributed, not to motion of an isolated fluoride anion, but rather to the total effect of all the mobile interstitial  $\text{F}^-$ , whose concentration is also activated. This may also explain the LiF prefactor, but it clearly does not apply to the extrinsic implanted  $^8\text{Li}^+$  in the dilute limit. With the advent of sensitive atomic resolution probes of surfaces in the past few decades, a very detailed picture of diffusion on crystal surfaces has emerged,<sup>92,93</sup> which can help to refine our ideas about bulk diffusion. For example, in some cases, the Arrhenius

prefactor of adatoms diffusing along a step edge is significantly enhanced over a flat terrace.<sup>94</sup> Like the channels in rutile, step edges consist of a 1D array of vacant sites, but the direct relevance is not clear, since the adatoms are generally far from the dilute limit. We suggest that most reasonable explanation of the high  $\tau_0^{-1}$  for long-range diffusion of  $\text{Li}^+$  in rutile is a large  $\Delta S$  which can result from a ballistic picture of hopping.<sup>86</sup> Similarly, a (Li/Ti) concentration dependence of  $\Delta S$  may contribute to the observed concentration dependence of  $D$ .<sup>2,19</sup>

A more common and widely discussed case is a small prefactor as we find at low temperature. Low prefactors are often encountered in superionic conductors both in NMR<sup>32,95</sup> and transport measurements, where they have been attributed to a breakdown of rate theory<sup>96</sup> or to low dimensionality that is often found for these structures<sup>97</sup> (the latter certainly applies to rutile). However, as argued above, the low temperature  $^8\text{Li}$  relaxation likely reflects polaron dynamics rather than  $\text{Li}^+$  motion. Evidence for this comes from the low temperature evolution of the electronic conductivity of lightly deoxidized rutile that shows a resistivity minimum at about 50 K.<sup>80</sup> The complex low temperature behavior of rutile probably combines polaron binding to defects<sup>79,80</sup> with intrinsic polaronic conductivity and the instability to delocalize.<sup>26</sup> Prefactors for defect-bound polarons at low temperature are significantly lower than our  $\tau_0^{-1}$ .<sup>79</sup> It would be interesting to compare our prefactor with the activated disappearance of the EPR<sup>25,29</sup> to test the connection between these two phenomena with very similar activation energies.

## V. CONCLUSION

In summary, using low-energy ion-implanted  $^8\text{Li}$   $\beta$ -NMR, we have studied the dynamics of isolated  $^8\text{Li}^+$  in rutile  $\text{TiO}_2$ . Two sets of thermally activated dynamics were found: one below 100 K; and one at higher-temperatures. At low temperature, an activation barrier of 26.8(6) meV is measured with an associated prefactor of  $1.23(5) \times 10^{10} \text{ s}^{-1}$ . We suggest this is unrelated to  $\text{Li}^+$  motion, and rather is a consequence of electron polarons in the vicinity of the implanted  $^8\text{Li}^+$  that are known to become mobile in this temperature range. Above 100 K,  $\text{Li}^+$  (not polaron complexed) undergoes long-range diffusion, characterized by an activation energy and prefactor of 0.32(2) eV and  $1.0(5) \times 10^{16} \text{ s}^{-1}$ , in agreement with macroscopic measurements. These results in the dilute limit from a microscopic probe indicate that  $\text{Li}^+$  concentration does not limit the diffusivity even up to high concentrations, but that some key ingredient is missing in the calculations of the barrier. Low temperature polaronic effects may also play a role in other titanate  $\text{Li}^+$  conductors, such as the perovskites<sup>98</sup> and spinels.<sup>99</sup> The present data, combined with EPR and transport studies, will further elucidate their properties.

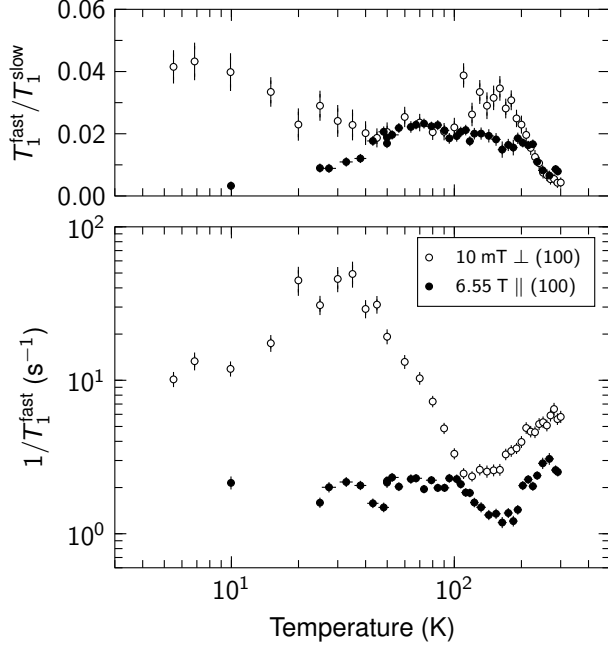


FIG. 8. Results from the analysis described in Section III A of the SLR measurements using Eq. 2 at high- and low-field. Shown are the ratio of the fast/slow relaxation times (top) and the fast relaxation rate (bottom). The ratio varies weakly with temperature and is field independent for much of it, deviating only in the vicinity of  $T_1^{\text{slow}}(T_{\text{min}})$ . Some of the features clearly seen in  $1/T_1^{\text{slow}}$  are apparent in  $1/T_1^{\text{fast}}$  (cf. Fig. 2), but much less pronounced, especially at high field.

### Appendix A: Biexponential Relaxation

Following the analysis described in Section III A, the fast relaxing component extracted from fitting the SLR measurements at high- and low-field to a biexponential relaxation [Eq. (2)] is shown in Fig. 8. While some of the qualitative features seen in the slow component at low temperatures are apparent in  $1/T_1^{\text{fast}}$ , they are much less pronounced at high field (see Fig. 3). The monotonic increase in  $1/T_1^{\text{fast}}$  above  $\sim 150$  K contrasts the behaviour of the slow component and dominates over any local maxima that may be present. Interestingly, the ratio of relaxation times  $T_1^{\text{fast}}/T_1^{\text{slow}}$  varies only weakly with temperature and remains field-independent over much of the temperature range. Deviations from a field-independent ratio occur near the local maxima in  $1/T_1^{\text{slow}}$ , clearly visible in Fig. 3.

We now consider what might produce the biexponential relaxation  $R(t, t')$  [Eq. (2)]. A fraction of the implanted  $^8\text{Li}^+$  stopping at a metastable crystallographic site at low temperature would show distinct resonance and relaxation, e.g.,  $^8\text{Li}^+$  in simple metals.<sup>60</sup> This would, however, be independent of applied field and would exhibit a very different temperature dependence from the in-channel diffusing site. As we find no clear evidence for multiple sites in the resonance analysis or field-

independent activated modulation of the SLR rates, we conclude a secondary site cannot be the source of the biexponential relaxation.

If quadrupolar fluctuations are the dominant source of relaxation, as would be expected for  $^8\text{Li}^+$  diffusion, then on the low temperature side of the  $T_1$  minimum, where the fluctuations are slow compared to  $\omega_L$ , the relaxation may be intrinsically biexponential for spin  $I = 2$ .<sup>58,59</sup> However, these Redfield-theory calculations of  $R(t, t')$  differ in several key assumptions from our situation, specifically: 1) the initial state of the optically polarized  $^8\text{Li}$  spin is quite different;<sup>47</sup> 2) we are not always in the extreme high field limit; and 3) one dimensional hopping yields a non-Debye fluctuation spectrum.<sup>67,68</sup> Moreover, above the  $T_1$  minimum, where the fluctuations are fast, the biexponential should collapse to a single exponential,<sup>58</sup> which is certainly not the case here, particularly for the low field data. It remains to be seen whether a suitably modified theory along these lines could account for the field dependence of the biexponential at high temperatures.

In contrast, at low temperature, we suspect the relaxation has a significant, possibly dominant, contribution from the polaron magnetic moment. Here, the spectrum of magnetic field fluctuations is naturally field dependent, yielding a strongly field dependent  $\lambda$ . In this case, some of the fast component at low fields would cross over to the high field slow component as  $\lambda(B_0)$  decreases with increasing field. A detailed field dependence of the relaxation at low field would help to confirm this. The character of the relaxation (magnetic, quadrupolar or mixed) can also be tested by comparison with another Li isotope, such as the spin  $3/2$   $^9\text{Li}$  as has been recently demonstrated.<sup>100</sup> It is important to recall that the amplitude of the relaxing signal is temperature independent even at low field, meaning that we do not have a fraction of the signal that is so fast relaxing that it is lost (wiped out) as has been seen in  $^7\text{Li}$  NMR from polarons in the perovskite  $\text{Li}_{3x}\text{La}_{2/3-x}\text{TiO}_3$ .<sup>98</sup> Thus if a significant fraction of  $^8\text{Li}^+$  forms the bound complex here, then its relaxation remains measurable even at low field.

### Appendix B: The 4c Site

The quadrupole splittings depend sensitively on the  $^8\text{Li}^+$  site and its symmetry, and with the angular dependence of the splittings [Eqs. (3), (4), and (5)] combined with calculations of the EFG (including lattice relaxation), one might be able to make a site assignment. Here we set out a few properties of the most likely site (4c) to make some initial observations based on the site symmetry in an ideal lattice.

The 4c site is coordinated by two near-neighbour and four more distant oxide ions in a shortened octahedron. As can be seen in Fig. 9A, the axis of the two nearest-neighbour oxide ions alternates from one site to the next along  $c$  by  $90^\circ$ . Beyond the first coordination, there

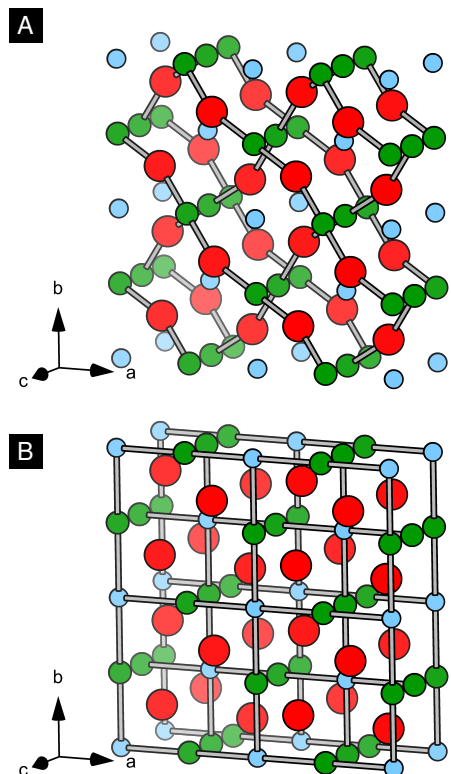


FIG. 9. View of the near-neighbour atoms to lithium(green) in the 4c site, showing their  $90^\circ$  alternating coordination axis between neighbouring 4c sites along the  $c$ -axis channels. The nearest-neighbour atoms are indicated here by connecting grey cylinders. (A) The two nearest-neighbour oxygen(red) atoms. (B) Two nearest-neighbour titanium(blue) atoms.

are two nearest neighbour Ti on opposite sides, and the Ti–Li–Ti direction also alternates between  $[100]$  and  $[010]$  along the channel, shown in Fig. 9B. Overall, the

site has  $2/m$  symmetry with the two-fold axis parallel to  $c$ . This symmetry is too low to yield an axial EFG, so  $\eta$  is nonzero, and may even approach 1; however, if we consider fast hopping along the  $c$ -axis, and the alternating character of the adjacent sites, one expects that the time-average EFG will become (four-fold) axisymmetric. This should be the case at room temperature, where there is clear evidence for  $\text{Li}^+$  diffusion, and a simple test of an axial angle dependence could confirm this.

The characteristics of this site are also important in determining properties of the  $\text{Li}^+$ -polaron complex. Here, one of the two neighbouring titanium is  $3+$ , rather than  $4+$ , which further lowers the site symmetry and alters the EFG. Calculations suggest that the polaron is mainly mobile along the stacks of adjacent edge-sharing  $\text{TiO}_6$  octahedra in the  $c$  direction<sup>12,23,26,27</sup> and it is unable to move to the other Ti neighbour on the far side of the Li site. Notice that if the polaron does hop to the next Ti along the stack, it is not the near neighbour of the adjacent Li site, but of the second nearest Li site along the chain. This is easily seen by the alternation of Ti–Li–Ti mentioned above (see Fig. 9B). If the bound complex moves in tandem, with the polaron remaining in a single  $\text{TiO}_6$  stack, then fast motional averaging should not result in an axisymmetric EFG, in contrast to the case of free  $\text{Li}^+$  diffusion.

## ACKNOWLEDGMENTS

We thank R. Abasalti, P.-A. Amaudruz, D.J. Arsenau, S. Daviel, B. Hitti, and D. Vyas for their excellent technical support. This work was supported by NSERC Discovery grants to R.F.K. and W.A.M. R.M.L.M. and A.C. acknowledge the additional support of their NSERC CREATE IsoSiM Fellowships. Crystal structure images were generated using CrystalMaker<sup>®</sup>: a crystal and molecular structures program for Mac and Windows. CrystalMaker Software Ltd, Oxford, England ([www.crystallmaker.com](http://www.crystallmaker.com)).

\* [rmlm@chem.ubc.ca](mailto:rmlm@chem.ubc.ca)

<sup>†</sup> Current address: Research School of Chemistry, Australian National University, Canberra, ACT 2601, Australia

<sup>‡</sup> Current address: School of Physical Science and Technology, ShanghaiTech University, Pudong, Shanghai 201210, China

<sup>§</sup> Current address: Heraeus Deutschland GmbH & Co. KG, Heraeusstraße 12–14, 63450 Hanau, Germany

<sup>¶</sup> [wam@chem.ubc.ca](mailto:wam@chem.ubc.ca)

<sup>1</sup> James A. Van Orman and Katherine L. Crispin, “Diffusion in oxides,” *Rev. Mineral. Geochem.* **72**, 757–825 (2010).

<sup>2</sup> O. W. Johnson, “One-dimensional diffusion of Li in rutile,” *Phys. Rev.* **136**, A284–A290 (1964).

<sup>3</sup> Philippe Knauth, “Inorganic solid Li ion conductors: An

overview,” *Solid State Ionics* **180**, 911–916 (2009).

<sup>4</sup> John Christopher Bachman, Sokseihua Muy, Alexis Gri-maud, Hao-Hsun Chang, Nir Pour, Simon F. Lux, Odysseas Paschos, Filippo Maglia, Saskia Lupart, Peter Lamp, Livia Giordano, and Yang Shao-Horn, “Inorganic solid-state electrolytes for lithium batteries: Mechanisms and properties governing ion conduction,” *Chem. Rev.* **116**, 140–162 (2016).

<sup>5</sup> Jeremy K. Burdett, Timothy Hughbanks, Gordon J. Miller, James W. Richardson Jr., and Joseph V. Smith, “Structural-electronic relationships in inorganic solids: powder neutron diffraction studies of the rutile and anatase polymorphs of titanium dioxide at 15 and 295 K,” *J. Am. Chem. Soc.* **109**, 3639–3646 (1987).

<sup>6</sup> M. V. Reddy, G. V. Subba Rao, and B. V. R. Chowdari, “Metal oxides and oxyalts as anode materials for Li ion

- batteries,” *Chem. Rev.* **113**, 5364–5457 (2013).
- <sup>7</sup> Y.-S. Hu, L. Kienle, Y.-G. Guo, and J. Maier, “High lithium electroactivity of nanometer-sized rutile  $\text{TiO}_2$ ,” *Adv. Mater.* **18**, 1421–1426 (2006).
  - <sup>8</sup> Marina V. Koudriachova, Nicholas M. Harrison, and Simon W. de Leeuw, “Effect of diffusion on lithium intercalation in titanium dioxide,” *Phys. Rev. Lett.* **86**, 1275–1278 (2001).
  - <sup>9</sup> Marina V. Koudriachova, Nicholas M. Harrison, and Simon W. de Leeuw, “Density-functional simulations of lithium intercalation in rutile,” *Phys. Rev. B* **65**, 235423 (2002).
  - <sup>10</sup> Marina V. Koudriachova, Nicholas M. Harrison, and Simon W. de Leeuw, “Diffusion of Li-ions in rutile. an ab initio study,” *Solid State Ionics* **157**, 35–38 (2003).
  - <sup>11</sup> F. Gligor and S. W. de Leeuw, “Lithium diffusion in rutile structured titania,” *Solid State Ionics* **177**, 2741–2746 (2006).
  - <sup>12</sup> Sebastien Kerisit, Kevin M. Rosso, Zhenguo Yang, and Jun Liu, “Dynamics of coupled lithium/electron diffusion in  $\text{TiO}_2$  polymorphs,” *J. Phys. Chem. C* **113**, 20998–21007 (2009).
  - <sup>13</sup> Peter V. Sushko, Kevin M. Rosso, and Igor V. Abarenkov, “Interaction of intercalated  $\text{Li}^+$  ions with oxygen vacancies in rutile  $\text{TiO}_2$ ,” *ECS Trans.* **28**, 299–306 (2010).
  - <sup>14</sup> Handan Yildirim, Jeffrey P. Greeley, and Subramanian K. R. S. Sankaranarayanan, “The effect of concentration on Li diffusivity and conductivity in rutile  $\text{TiO}_2$ ,” *Phys. Chem. Chem. Phys.* **14**, 4565–4576 (2012).
  - <sup>15</sup> Sebastien Kerisit, Anne M. Chaka, Timothy C. Droubay, and Eugene S. Ilton, “Shell model for atomistic simulation of lithium diffusion in mixed Mn/Ti oxides,” *J. Phys. Chem. C* **118**, 24231–24239 (2014).
  - <sup>16</sup> Jongbo Jung, Maenghyo Cho, and Min Zhou, “Density functional theory study of the mechanism of Li diffusion in rutile  $\text{RuO}_2$ ,” *AIP Adv.* **4**, 017104 (2014).
  - <sup>17</sup> Jayeon Baek, Soomin Park, Chyan Kyung Song, Tae Yong Kim, Inho Nam, Jong Min Lee, Jeong Woo Han, and Jongheop Yi, “Radial alignment of  $c$ -channel nanorods in 3D porous  $\text{TiO}_2$  for eliciting enhanced Li storage performance,” *Chem. Commun.* **51**, 15019–15022 (2015).
  - <sup>18</sup> Corinne Arrouvel, Thiago C. Peixoto, Mario E. G. Valerio, and Stephen C. Parker, “Lithium migration at low concentration in  $\text{TiO}_2$  polymorphs,” *Comput. Theor. Chem.* **1072**, 43–51 (2015).
  - <sup>19</sup> S. Bach, J. P. Pereira-Ramos, and P. Willman, “Investigation of lithium diffusion in nano-sized rutile  $\text{TiO}_2$  by impedance spectroscopy,” *Electrochim. Acta.* **55**, 4952–4959 (2010).
  - <sup>20</sup> J. Heine, M. Wilkening, and P. Heitjans, “Slow  $\text{Li}^+$  self-diffusion in Li intercalated nanometer-sized needlelike rutile  $\text{TiO}_2$  as probed by mixing time dependent  $^7\text{Li}$  stimulated echo NMR spectroscopy,” *Diffus. Fundament.* **12**, 95–96 (2010).
  - <sup>21</sup> Martin Setvin, Cesare Franchini, Xianfeng Hao, Michael Schmid, Anderson Janotti, Merzuk Kaltak, Chris G. Van de Walle, Georg Kresse, and Ulrike Diebold, “Direct view at excess electrons in  $\text{TiO}_2$  rutile and anatase,” *Phys. Rev. Lett.* **113**, 086402 (2014).
  - <sup>22</sup> Krzysztof Szot, Gustav Bihlmayer, and Wolfgang Speier, “Nature of the resistive switching phenomena in  $\text{TiO}_2$  and  $\text{SrTiO}_3$ : Origin of the reversible insulator-metal transition,” in *Solid State Physics*, Vol. 65, edited by Robert E. Camley and Robert L. Stamps (Academic Press, 2014) Chap. 4, pp. 353–559.
  - <sup>23</sup> N. Aaron Deskins and Michel Dupuis, “Electron transport via polaron hopping in bulk  $\text{TiO}_2$ : A density functional theory characterization,” *Phys. Rev. B* **75**, 195212 (2007).
  - <sup>24</sup> Hikmet Sezen, Maria Buchholz, Alexei Nefedov, Carsten Natzeck, Stefan Heissler, Cristiana Di Valentin, and Christof Wöll, “Probing electrons in  $\text{TiO}_2$  polaronic trap states by IR-absorption: Evidence for the existence of hydrogenic states,” *Sci. Rep.* **4**, 3808 (2014).
  - <sup>25</sup> Shan Yang, A. T. Brant, N. C. Giles, and L. E. Halliburton, “Intrinsic small polarons in rutile  $\text{TiO}_2$ ,” *Phys. Rev. B* **87**, 125201 (2013).
  - <sup>26</sup> A. Janotti, C. Franchini, J. B. Varley, G. Kresse, and C. G. Van de Walle, “Dual behavior of excess electrons in rutile  $\text{TiO}_2$ ,” *Phys. Status Solidi RRL* **7**, 199–203 (2013).
  - <sup>27</sup> Likai Yan, Justin E. Elenewski, Wei Jiang, and Hanning Chen, “Computational modeling of self-trapped electrons in rutile  $\text{TiO}_2$ ,” *Phys. Chem. Chem. Phys.* **17**, 29949–29957 (2015).
  - <sup>28</sup> Ji-Yong Shin, Dominik Samuelis, and Joachim Maier, “Defect chemistry of lithium storage in  $\text{TiO}_2$  as a function of oxygen stoichiometry,” *Solid State Ionics* **225**, 590–593 (2012).
  - <sup>29</sup> A. T. Brant, N. C. Giles, and L. E. Halliburton, “Insertion of lithium ions into  $\text{TiO}_2$  (rutile) crystals: An electron paramagnetic resonance study of the Li-associated  $\text{Ti}^{3+}$  small polaron,” *J. Appl. Phys.* **113**, 053712 (2013).
  - <sup>30</sup> Jianguo Yu, Maria L. Sushko, Sebastien Kerisit, Kevin M. Rosso, and Jun Liu, “Kinetic Monte Carlo study of ambipolar lithium ion and electron-polaron diffusion into nanostructured  $\text{TiO}_2$ ,” *J. Phys. Chem. Lett.* **3**, 2076–2081 (2012).
  - <sup>31</sup> N. Bloembergen, E. M. Purcell, and R. V. Pound, “Relaxation effects in nuclear magnetic resonance absorption,” *Phys. Rev.* **73**, 679–712 (1948).
  - <sup>32</sup> P. M. Richards, “Magnetic resonance in superionic conductors,” in *Physics of Superionic Conductors*, Topics in Current Physics, Vol. 15, edited by Myron B. Salamon (Springer, 1979) Chap. 6, pp. 141–174.
  - <sup>33</sup> O. Kanert, “Dynamical properties of defects in solids,” *Phys. Rep.* **91**, 183–232 (1982).
  - <sup>34</sup> Detlef Brinkmann, “NMR studies of superionic conductors,” *Prog. Nucl. Magn. Reson. Spectrosc.* **24**, 527–552 (1992).
  - <sup>35</sup> Paul Heitjans, Andreas Schirmer, and Sylvio Indris, “NMR and  $\beta$ -NMR studies of diffusion in interface-dominated and disordered solids,” in *Diffusion in Condensed Matter*, edited by Paul Heitjans and Jörg Kärger (Springer, 2005) 2nd ed., Chap. 9, pp. 367–415.
  - <sup>36</sup> R. Böhmer, K. R. Jeffrey, and M. Vogel, “Solid-state Li NMR with applications to the translational dynamics in ion conductors,” *Prog. Nucl. Magn. Reson. Spectrosc.* **50**, 87–174 (2007).
  - <sup>37</sup> A. Kuhn, M. Kunze, P. Sreeraj, H.-D. Wiemhöfer, V. Thangadurai, M. Wilkening, and P. Heitjans, “NMR relaxometry as a versatile tool to study Li ion dynamics in potential battery materials,” *Solid State Nucl. Magn. Reson.* **42**, 2–8 (2012).
  - <sup>38</sup> Martin Wilkening and Paul Heitjans, “From micro to macro: Access to long-range  $\text{Li}^+$  diffusion parameters in solids via microscopic  $^6,^7\text{Li}$  spin-alignment echo NMR spectroscopy,” *ChemPhysChem* **13**, 53–65 (2012).
  - <sup>39</sup> C. Vinod Chandran and P. Heitjans, “Solid-state NMR studies of lithium ion dynamics across materials classes,”

- in *Annual Reports on NMR Spectroscopy*, Vol. 89, edited by Graham A. Webb (Academic Press, 2016) Chap. 1, pp. 1–102.
- <sup>40</sup> H. Ackermann, P. Heitjans, and H.-J. Stöckmann, “ $\beta$  emitters and isomeric nuclei as probes in condensed matter,” in *Hyperfine Interactions of Radioactive Nuclei*, Topics in Current Physics, Vol. 31, edited by Jens Christiansen (Springer, 1983) Chap. 6, pp. 291–361.
  - <sup>41</sup> W. A. MacFarlane, “Implanted-ion  $\beta$ NMR: A new probe for nanoscience,” *Solid State Nucl. Magn. Reson.* **68–69**, 1–12 (2015).
  - <sup>42</sup> G. D. Morris, W. A. MacFarlane, K. H. Chow, Z. Salman, D. J. Arseneau, S. Daviel, A. Hatakeyama, S. R. Kreitzman, C. D. P. Levy, R. Poutissou, R. H. Heffner, J. E. Elenewski, L. H. Greene, and R. F. Kiefl, “Depth-controlled  $\beta$ -NMR of  $^8\text{Li}$  in a thin silver film,” *Phys. Rev. Lett.* **93**, 157601 (2004).
  - <sup>43</sup> Z. Salman, E. P. Reynard, W. A. MacFarlane, K. H. Chow, J. Chakhalian, S. R. Kreitzman, S. Daviel, C. D. P. Levy, R. Poutissou, and R. F. Kiefl, “ $\beta$ -detected nuclear quadrupole resonance with a low-energy beam of  $^8\text{Li}^+$ ,” *Phys. Rev. B* **70**, 104404 (2004).
  - <sup>44</sup> Gerald D. Morris, “ $\beta$ -NMR,” *Hyperfine Interact.* **225**, 173–182 (2014).
  - <sup>45</sup> R. M. L. McFadden, D. L. Cortie, D. J. Arseneau, T. J. Buck, C.-C. Chen, M. H. Dehn, S. R. Dunsiger, R. F. Kiefl, C. D. P. Levy, C. Li, G. D. Morris, M. R. Pearson, D. Samuelis, J. Xiao, J. Maier, and W. A. MacFarlane, “ $\beta$ -NMR of  $^8\text{Li}^+$  in rutile  $\text{TiO}_2$ ,” *J. Phys.: Conf. Ser.* **551**, 012032 (2014).
  - <sup>46</sup> James F. Ziegler, Jochen P. Biersack, and Matthias D. Ziegler, *SRIM — The Stopping and Range of Ions in Matter*, 7th ed. (SRIM Co., 2008) <http://www.srim.org/>.
  - <sup>47</sup> W. A. MacFarlane, C. D. P. Levy, M. R. Pearson, T. Buck, K. H. Chow, A. N. Hariwal, R. F. Kiefl, F. H. McGee, G. D. Morris, and D. Wang, “The initial state of optically polarized  $^8\text{Li}^+$  from the  $\beta$ -NMR in bismuth,” *J. Phys.: Conf. Ser.* **551**, 012059 (2014).
  - <sup>48</sup> M. E. Straumanis, T. Ejima, and W. J. James, “The  $\text{TiO}_2$  phase explored by the lattice constant and density method,” *Acta Cryst.* **14**, 493–497 (1961).
  - <sup>49</sup> Z. Salman, R. F. Kiefl, K. H. Chow, M. D. Hossain, T. A. Keeler, S. R. Kreitzman, C. D. P. Levy, R. I. Miller, T. J. Parolin, M. R. Pearson, H. Saadaoui, J. D. Schultz, M. Smadella, D. Wang, and W. A. MacFarlane, “Near-surface structural phase transition of  $\text{SrTiO}_3$  studied with zero-field  $\beta$ -detected nuclear spin relaxation and resonance,” *Phys. Rev. Lett.* **96**, 147601 (2006).
  - <sup>50</sup> W. A. MacFarlane, Q. Song, N. J. C. Ingle, K. H. Chow, M. Egilmez, I. Fan, M. D. Hossain, R. F. Kiefl, C. D. P. Levy, G. D. Morris, T. J. Parolin, M. R. Pearson, H. Saadaoui, Z. Salman, and D. Wang, “ $\beta$ -detected NMR spin relaxation in a thin film heterostructure of ferromagnetic  $\text{EuO}$ ,” *Phys. Rev. B* **92**, 064409 (2015).
  - <sup>51</sup> W. A. MacFarlane, T. J. Parolin, D. L. Cortie, K. H. Chow, M. D. Hossain, R. F. Kiefl, C. D. P. Levy, R. M. L. McFadden, G. D. Morris, M. R. Pearson, H. Saadaoui, Z. Salman, Q. Song, and D. Wang, “ $^8\text{Li}^+$   $\beta$ -NMR in the cubic insulator  $\text{MgO}$ ,” *J. Phys.: Conf. Ser.* **551**, 012033 (2014).
  - <sup>52</sup> W. A. MacFarlane, G. D. Morris, K. H. Chow, R. A. Baartman, S. Daviel, S. R. Dunsiger, A. Hatakeyama, S. R. Kreitzman, C. D. P. Levy, R. I. Miller, K. M. Nichol, R. Poutissou, E. Dumont, L. H. Greene, and R. F. Kiefl, “Quadrupolar split  $^8\text{Li}$   $\beta$ -NMR in  $\text{SrTiO}_3$ ,” *Physica B* **326**, 209–212 (2003).
  - <sup>53</sup> V. L. Karner *et al.*, to be published.
  - <sup>54</sup> M. Ogura, K. Minamisono, T. Sumikama, T. Nagatomo, T. Iwakoshi, T. Miyake, K. Hashimoto, S. Kudo, K. Arimura, M. Ota, K. Akutsu, K. Sato, M. Mihara, M. Fukuda, K. Matsuta, H. Akai, and T. Minamisono, “A possible nuclear spin dewar. hyperfine interactions of short-lived  $\beta$  emitter  $^8\text{Li}$  and  $^{12}\text{B}$  in  $\text{TiO}_2$ ,” *Hyperfine Interact.* **136**, 195–199 (2001).
  - <sup>55</sup> F. James and M. Roos, “MINUIT — a system for function minimization and analysis of the parameter errors and correlations,” *Comput. Phys. Commun.* **10**, 343–367 (1975).
  - <sup>56</sup> Rene Brun and Fons Rademakers, “ROOT — an object oriented data analysis framework,” *Nucl. Instrum. Methods Phys. Res., Sect. A* **389**, 81–86 (1997), <https://root.cern.ch/>.
  - <sup>57</sup> Paul S. Hubbard, “Nonexponential nuclear magnetic relaxation by quadrupole interactions,” *J. Chem. Phys.* **53**, 985–987 (1970).
  - <sup>58</sup> K. D. Becker, “Nuclear magnetic relaxation induced by the dynamics of lattice defects in solids ( $I = 3/2$ ,  $I = 2$ , and  $I = 5/2$ ),” *Z. Naturforsch. A* **37**, 697–705 (1982).
  - <sup>59</sup> A. Körblein, P. Heitjans, H.-J. Stöckmann, F. Fujara, H. Ackermann, W. Buttler, K. Dörr, and H. Grupp, “Diffusion processes in solid Li-Mg and Li-Ag alloys and the spin-lattice relaxation of  $^8\text{Li}$ ,” *J. Phys. F: Met. Phys.* **15**, 561–577 (1985).
  - <sup>60</sup> M. D. Hossain, H. Saadaoui, T. J. Parolin, Q. Song, D. Wang, M. Smadella, K. H. Chow, M. Egilmez, I. Fan, R. F. Kiefl, S. R. Kreitzman, C. D. P. Levy, G. D. Morris, M. R. Pearson, Z. Salman, and W. A. MacFarlane, “The spin lattice relaxation of  $^8\text{Li}$  in simple metals,” *Physica B* **404**, 914–916 (2009).
  - <sup>61</sup> M. H. Cohen and F. Reif, “Quadrupole effects in nuclear magnetic resonance studies of solids,” in *Solid State Physics*, Vol. 5, edited by Frederick Seitz and David Turnbull (Academic Press, 1957) pp. 321–438.
  - <sup>62</sup> Miroslav Morháč, Ján Kliman, Vladislav Matoušek, Martin Veselský, and Ivan Turzo, “Background elimination methods for multidimensional coincidence  $\gamma$ -ray spectra,” *Nucl. Instrum. Methods Phys. Res., Sect. A* **401**, 113–132 (1997).
  - <sup>63</sup> B. Jansen-Glaw, E. Rössler, M. Taupitz, and H.M. Vieth, “Hexamethylbenzene as a sensitive nuclear magnetic resonance probe for studying organic crystals and glasses,” *J. Chem. Phys.* **90**, 6858–6866 (1989).
  - <sup>64</sup> Alexander Kuhn, Viola Duppel, and Bettina V. Lotsch, “Tetragonal  $\text{Li}_{10}\text{GeP}_2\text{S}_{12}$  and  $\text{Li}_7\text{GePS}_8$  — exploring the Li ion dynamics in LGPS Li electrolytes,” *Energy Environ. Sci.* **6**, 3548–3552 (2013).
  - <sup>65</sup> Peter A. Beckmann, “Spectral densities and nuclear spin relaxation in solids,” *Phys. Rep.* **171**, 85–128 (1988).
  - <sup>66</sup> C. A. Sholl, “Nuclear spin relaxation by translational diffusion in liquids and solids: high- and low-frequency limits,” *J. Phys. C: Solid State Phys* **14**, 447–464 (1981).
  - <sup>67</sup> Peter A. Fedders, “Dynamic quadrupole nuclear-spin relaxation of deuterium in metals in the  $\alpha$  or  $\alpha'$  phases,” *Phys. Rev. B* **15**, 2500–2503 (1977).
  - <sup>68</sup> Peter A. Fedders, “Moment expansions and occupancy (site) correlation functions for a one-dimensional hopping,” *Phys. Rev. B* **17**, 2098–2109 (1978).

- <sup>69</sup> R. Messer, H. Birli, and K. Differt, “NMR study of diffusion in  $\text{Li}_3\text{N}$ ,” *J. Phys. C: Solid State Phys.* **14**, 2731 (1981).
- <sup>70</sup> A. V. Churikov, V. A. Zobenkova, and K. I. Pridatko, “Lithium intercalation into titanium dioxide films from a propylene carbonate solution,” *Russ. J. Electrochem.* **40**, 63–68 (2004).
- <sup>71</sup> A. V. Churikov, A. V. Ivanishchev, A. V. Ushakov, and V. O. Romanova, “Diffusion aspects of lithium intercalation as applied to the development of electrode materials for lithium-ion batteries,” *J. Solid State Electrochem.* **18**, 1425–1441 (2014).
- <sup>72</sup> Rebecca A. Parker, “Static dielectric constant of rutile ( $\text{TiO}_2$ ), 1.6–1060°K,” *Phys. Rev.* **124**, 1719–1722 (1961).
- <sup>73</sup> Helmut Mehrer, “Correlation in solid-state diffusion,” in *Diffusion in Solids: Fundamentals, Methods, Materials, Diffusion-Controlled Processes*, Springer Series in Solid-State Sciences, Vol. 155 (Springer, 2007) Chap. 7, pp. 105–125.
- <sup>74</sup> O. W. Johnson and H. R. Krouse, “Isotopic mass dependence of Li diffusion in rutile,” *J. Appl. Phys.* **37**, 668–670 (1966).
- <sup>75</sup> W. Müller-Warmuth, “NMR studies of guest molecules in intercalation compounds,” *Colloids Surf.* **11**, 1–17 (1984).
- <sup>76</sup> Wouter J. H. Borghols, Marnix Wagemaker, Ugo Lafont, Erik M. Kelder, and Fokko M. Mulder, “Impact of nano-sizing on lithiated rutile  $\text{TiO}_2$ ,” *Chem. Mater.* **20**, 2949–2955 (2008).
- <sup>77</sup> M. Vijayakumar, Sebastien Kerisit, Chongmin Wang, Zimin Nie, Kevin M. Rosso, Zhenguo Yang, Gordon Graff, Jun Liu, and Jianzhi Hu, “Effect of chemical lithium insertion into rutile  $\text{TiO}_2$  nanorods,” *J. Phys. Chem. C* **113**, 14567–14574 (2009).
- <sup>78</sup> R. D. Shannon, “Revised effective ionic radii and systematic studies of interatomic distances in halides and chalcogenides,” *Acta Cryst.* **A32**, 751–767 (1976).
- <sup>79</sup> L. A. K. Dominik and R. K. MacCrone, “Dielectric relaxations in reduced rutile ( $\text{TiO}_{2-x}$ ) at low temperatures,” *Phys. Rev.* **163**, 756–768 (1967).
- <sup>80</sup> Eiichi Yagi, Ryukiti R. Hasiguti, and Masakazu Aono, “Electronic conduction above 4 K of slightly reduced oxygen-deficient rutile  $\text{TiO}_{2-x}$ ,” *Phys. Rev. B* **54**, 7945–7956 (1996).
- <sup>81</sup> S. R. Kreitzman, “RF resonance techniques for continuous muon beams,” *Hyperfine Interact.* **65**, 1055–1069 (1991).
- <sup>82</sup> S. R. Kreitzman, B. Hitti, R. L. Lichti, T. L. Estle, and K. H. Chow, “Muon-spin-resonance study of muonium dynamics in Si and its relevance to hydrogen,” *Phys. Rev. B* **51**, 13117–13137 (1995).
- <sup>83</sup> Marco Villa and John L. Bjorkstam, “Prefactor anomalies,” *Solid State Ionics* **9**, 1421–1426 (1983).
- <sup>84</sup> C. Wert and C. Zener, “Interstitial atomic diffusion coefficients,” *Phys. Rev.* **76**, 1169–1175 (1949).
- <sup>85</sup> George H. Vineyard, “Frequency factors and isotope effects in solid state rate processes,” *J. Phys. Chem. Solids* **3**, 121–127 (1957).
- <sup>86</sup> T. W. Dobson, J. F. Wager, and J. A. Van Vechten, “Entropy of migration for atomic hopping,” *Phys. Rev. B* **40**, 2962–2967 (1989).
- <sup>87</sup> D. P. Almond and A. R. West, “The activation entropy for transport in ionic conductors,” *Solid State Ionics* **23**, 27–35 (1987).
- <sup>88</sup> A. Yelon, B. Movaghar, and H. M. Branz, “Origin and consequences of the compensation (Meyer-Neldel) law,” *Phys. Rev. B* **46**, 12244–12250 (1992).
- <sup>89</sup> A. Yelon, B. Movaghar, and R. S. Crandall, “Multi-excitation entropy: its role in thermodynamics and kinetics,” *Rep. Prog. Phys.* **69**, 1145–1194 (2006).
- <sup>90</sup> Maurice Eisenstadt, “Nuclear magnetic relaxation in  $\text{LiF}$  at high temperatures,” *Phys. Rev.* **132**, 630–635 (1963).
- <sup>91</sup> J. B. Boyce, J. C. Mikkelsen, and M. O’Keeffe, “Ion dynamics and sublattice melting in the superionic conductor  $\text{PbF}_2$ ,” *Solid State Commun.* **21**, 955–958 (1977).
- <sup>92</sup> Michael C. Tringides and Myron Hupalo, “Fluctuations and growth phenomena in surface diffusion,” in *Diffusion in Condensed Matter*, edited by Paul Heitjans and Jörg Kärger (Springer, 2005) 2nd ed., Chap. 7, pp. 285–335.
- <sup>93</sup> Grazyna Antczak and Gert Ehrlich, “Jump processes in surface diffusion,” *Surf. Sci. Rep.* **62**, 39–61 (2007).
- <sup>94</sup> Holger Röder, Karsten Bromann, Harald Brune, and Klaus Kern, “Diffusion-limited aggregation with active edge diffusion,” *Phys. Rev. Lett.* **74**, 3217–3220 (1995).
- <sup>95</sup> J. B. Boyce and B. A. Huberman, “Superionic conductors: Transitions, structures, dynamics,” *Phys. Rep.* **51**, 189–265 (1979).
- <sup>96</sup> B. A. Huberman and J. B. Boyce, “Breakdown of absolute rate theory and prefactor anomalies in superionic conductors,” *Solid State Commun.* **25**, 759–762 (1978).
- <sup>97</sup> Peter M. Richards, “Effect of low dimensionality on prefactor anomalies in superionic conductors,” *Solid State Commun.* **25**, 1019–1021 (1978).
- <sup>98</sup> J. Emery, O. Bohnke, J. L. Fourquet, J. Y. Buzaré, P. Florian, and D. Massiot, “Polaronic effects on lithium motion in intercalated perovskite lithium lanthanum titanate observed by  $^7\text{Li}$  NMR and impedance spectroscopy,” *J. Phys.: Condens. Matter* **11**, 10401–10417 (1999).
- <sup>99</sup> Jun Sugiyama, Izumi Umegaki, Takeshi Uyama, Ryan M. L. McFadden, Susumu Shiraki, Taro Hitosugi, Zaher Salman, Hassan Saadaoui, Gerald D. Morris, W. Andrew MacFarlane, and Robert F. Kiefl, “Lithium diffusion in spinel  $\text{Li}_4\text{Ti}_5\text{O}_{12}$  and  $\text{LiTi}_2\text{O}_4$  films detected with  $^8\text{Li}$   $\beta$ -NMR,” *Phys. Rev. B* **96**, 094402 (2017).
- <sup>100</sup> A. Chatzichristos, R. M. L. McFadden, V. L. Karner, D. L. Cortie, C. D. P. Levy, W. A. MacFarlane, G. D. Morris, M. R. Pearson, Z. Salman, and R. F. Kiefl, “Determination of the nature of fluctuations using  $^8\text{Li}$  and  $^9\text{Li}$   $\beta$ -NMR and spin-lattice relaxation,” *Phys. Rev. B* **96**, 014307 (2017).